Dynamical robustness of the conductivity of ultracold bosons confined in layered structures

A. S. Sajna and T. P. Polak

Solid State Theory Division, Faculty of Physics, A. Mickiewicz University, ul. Umultowska 85, 61-614 Poznań, Poland

(Received 31 March 2014; published 6 October 2014)

We study dynamical conductivity of strongly correlated bosons loaded in an optical lattice with restricted geometry in which gauge fields are present. We show that dynamics influenced by the uniform synthetic magnetic field combined with layered lattice structures changes into rich insulator-metallic behavior in the strongly correlated regime. Especially, the amplitude of optical conductivity for a given frequency is a nonmonotonous function of the number of layers L. In particular, conductivity for frequency corresponding to on-site interaction energy can abruptly vanish for a special number of applied layers. Moreover, such an insulating behavior is stable in the whole range of parameters in the Mott phase. This robustness arises from the complex gaplike behavior or from Dirac-like physics reflected in the quasiparticle energy spectra. Furthermore we show that a large interlayer tunneling anisotropy destabilizes the absence of conducting state. We also investigate the critical conductivity on the Mott-insulator–superfluid phase boundary and show the correspondence between the number of Hofstadter subbands and the number of layers. The obtained results also reveal that the value of critical conductivity gradually goes to zero when a three-dimensional system is approached. The experimental setup for generation of layered optical lattices is also proposed.

DOI: 10.1103/PhysRevA.90.043603 PACS number(s): 03.75.Lm, 05.30.Jp, 03.75.Nt

I. INTRODUCTION

The properties of matter depend on many different degrees of freedom. A set of such degrees of freedom that we shall be concerned with in this study is determined by the geometry of the system. Especially, lattice patterns or dimensionality have been widely studied theoretically and experimentally in the ultracold atomic systems [1–10]. But most of the studies have not dealt with the cases when discrete effects are important [11,12] (several layers were created, e.g., in Ref. [13]). Furthermore, no effective method for generation and control of such a restricted geometry with layered patterns has been proposed.

We show that optical lattices should be the perfect simulators of systems in which discrete and continuous transition from two dimensions (2D) to three dimensions (3D) can interplay. The experimental scheme proposed in this paper is not related to the internal structure of the atom [12,14] and should be treated as an extension of the experimental setups proposed so far (see, e.g., [15,16]). This motivated us to investigate the dynamics of ultracold atoms to show the richness of their behavior in such systems. Moreover, a variety of the types of dynamical behavior emerges especially when synthetic magnetic field effects, which are currently available in the experiments, are taken into account [17–19]. To do so, we apply the analytical methods for optical conductivity with the intra-Hofstadter-band transitions, developed in Ref. [20] for investigation of layered systems with tunneling anisotropy in the z direction, where the Hofstadter spectrum is split by the boson interaction energy. Conductivity in an optical lattice could be directly available as shown in recent experimental proposals [21,22].

Throughout this paper, we focus especially on strongly interacting bosons on the optical lattice described by the Bose-Hubbard model (BHM) [23]. Experiments and theory have shown that in the deep lattice regime ultracold atoms undergo a Mott-insulator–superfluid (MI-SF) transition and the quasiparticle spectrum acquires an energy gap [15,24–26]. The deep lattice regime in the zero temperature limit is a subject of our interest.

Moreover, we also study the critical phenomena related to the finite conductivity at the quantum phase transition in the 2D to 3D crossover region. From previous studies it is known that it acquires finite value only for two dimensions [27], while for three dimensions it disappears [28]. Such a behavior is a direct consequence of the vanishing engineering dimension of the conductivity [28], which makes the investigation of the crossover region more interesting. Besides, the critical conductivity analysis is also important because of its universal value, i.e., it is not dependent on BHM Hamiltonian parameters [27]. With these motivations, we show that the two- and three-dimensional limiting cases of the critical conductivity are recovered (Ref. [20] and references therein). In the intermediate region, we study its dependence on the number of layers.

The rest of the paper is organized as follows. In Sec. II we briefly describe the method applied. In Sec. III we study the impact of additional layers on the optical and the critical conductivity. In Sec. IV we propose an experimental setup. Finally, we give a summary of our work.

II. MODEL

In the following, we use the BHM to describe strongly correlated bosons on the lattice subjected to Abelian gauge fields, introduced by the Peierls factor $\exp(i\frac{e^*}{\hbar c}\int_j^i \mathbf{A}_0 \cdot d\mathbf{l})$. Although the charge of the bosons e^* in optical lattices is neutral, it could be effectively generated by engineering a vector potential $\mathbf{A}_0$ [29]. Moreover, the ground state of the BHM is controlled by three parameters: the hopping term J_{ij}, the on-site interaction energy U, and the chemical potential μ. These parameters within the BHM Hamiltonian are incorporated among the creation $b_i^\dagger$ and annihilation b_i boson operators (i denotes site index) and consequently BHM

Hamiltonian reads

$$H = -\sum_{\langle ij\rangle}\left(J_{ij}e^{i\frac{e^*}{\hbar c}\int_j^i \mathbf{A}_0\cdot d\mathbf{l}}\hat{b}_i^\dagger\hat{b}_j + \text{H.c.}\right) - \mu\sum_i \hat{n}_i + \frac{U}{2}\sum_i \hat{n}_i(\hat{n}_i - 1). \quad (1)$$

In this work, the hopping term $J_{ij} = J$ is nonzero only for nearest-neighbor lattice sites as stressed in Eq. (1) using parentheses $\langle\ldots\rangle$. The remaining notation used in Eq. (1) are the density operator $\hat{n}_i = b_i^\dagger b_i$, the reduced Planck constant $\hbar$, and speed of light c.

In order to study dynamical properties of the Mott-insulator (MI) state in the slab geometry, we use the coherent state path integral method. In this study we also include commensurability effects of magnetic fluxes. The method used here was developed in Refs. [20] and [11] (and references therein) so in the following we omit technical details.

If we are interested in strong orbital magnetic field effects it is useful to introduce the ratio $p/q = f$, where p and q are coprime integers. This ratio gives the information about the phase gained by bosons when they hop around the lattice cell. The quantity f is related to the previous parameters by $f = Ba^2e^*/hc$ where B is the amplitude of the uniform magnetic field obtained from the Landau gauge $\mathbf{A}_0 = B(0,x,0)$ with a being a lattice constant. To simplify the equations we set a, $\hbar$, and c to unity.

We focus now on the dynamics of BHM. This can be probed, e.g., by the time-dependent external electric field attached to the system. Then the induced charge current can be investigated through measurements of the frequency-dependent conductivity (e.g., using the energy absorption rate [21]). If the response is conducted in the linear regime we can use the magnetic Kubo formula proposed in Ref. [20] to express the real and regular part of optical conductivity (OC) in the Mott phase in the form

$$\mathrm{Re}\sigma_{xx}^{\mathbf{A}_0}(\omega) = 2\pi^2\sigma_Q\sum_\alpha\sum_{s=\{+,-\}}\Xi_q^\alpha[u^s(\omega);p], \quad (2)$$

$$\Xi_q^\alpha[v;p] = \rho_q^\alpha(v;p)\frac{J\left[z_q^\alpha(v;p)-1\right]z_q^\alpha(v;p)}{U\sqrt{4n_0(n_0+1)+(\omega/U)^2}}, \quad (3)$$

$$u^\pm(\omega) = \frac{U}{J}(2n_0+1)\left(1\mp\sqrt{1-\frac{1-(\omega/U)^2}{(2n_0+1)^2}}\right), \quad (4)$$

where the weighted density of states for conductivity (DOSc) is given by the formula

$$\rho_q^\alpha(v;p) = \frac{1}{N}\sum_{\mathbf{k}}\left[\partial_{k_x}\epsilon_q^\alpha(\mathbf{k};p)\right]^2\delta\left(v-\epsilon_q^\alpha(\mathbf{k};p)/J\right), \quad (5)$$

in which $\delta(x)$ is the Dirac δ function and $\sigma_Q = (e^*)^2/h$ is a quantum conductance. To be more specific, the form of $\mathrm{Re}\sigma_{xx}^{\mathbf{A}_0}(\omega)$ in Eq. (2) could be simply understood using spectral representation of current-current correlation function [20]. Namely, $\Xi_q^\alpha[v;p]$ is the spectral weight of OC with the energy range decoded in DOSc and $u^\pm(\omega)$ gives the normalized single-particle band energy for which this spectral weight appears (superscript $\pm$ denote lower and higher energy channel). Moreover, in Eq. (2), we take into account strong uniform magnetic field effects tuned by p/q ratio. The summation goes over the wave vector $\mathbf{k} = (k_x, k_y)$ ($|k_x| \le \pi/q, |k_x| \le \pi$). Furthermore, N is the number of sites in the lattice and n_0 is an integer number, which is equal to the average boson density per site in the Mott-insulator phase. In Eq. (5), for a given f, the single-particle energy dispersions are denoted by $\epsilon_q^\alpha(\mathbf{k};p)$ and each subband is numbered by $\alpha = 0, 1, 2, \ldots, q-1$. The weight $z_q^\alpha(v;p)$ is defined in details in Appendix A. It is worth to add here that α subbands can be obtained using the Harper equation [20,30]. In general, they follow from the standard considerations about tight binding dispersion but with additional difficulty, i.e., there is a phase acquired by bosons when they hop from site to site. As a consequence for square lattice, this phase introduces q different types of sites, which also causes q branches of excitation emerging here as $\epsilon_q^\alpha(\mathbf{k};p)$ subbands.

To investigate the effects resulting from the layered-like structure it is sufficient, by using the tight binding approximation [11] for three-dimensional lattice

$$\epsilon_{q,3D}^\alpha(\mathbf{k};p) = \epsilon_q^\alpha(\mathbf{k};p) - 2J_z\cos k_z, \quad (6)$$

to modify the DOSc presented in Eq. (5), namely

$$\rho_{q,3D}^\alpha(v;p) = \frac{1}{L}\sum_{k_z}\rho_q^\alpha(v+2\eta\cos k_z;p), \quad (7)$$

where L denotes the number of layers parallel to the xy plane (for derivation details see Appendix B) and $k_z = 2\pi m/L$ with $m \in \{0, 1, \ldots, L-1\}$. Parameter η controls the anisotropy in z direction, i.e., $\eta = J_z/J$.

III. RESULTS

A. Dynamical conductivity in layered structure

In Ref. [20] it has been shown that for two-dimensional systems, OC abruptly changes, showing the Hofstadter-like structure [31]. In other words, the subbands presented in the Hofstadter spectrum are reflected by the pronounced peaks in the frequency-dependent optical conductivity. Moreover the center of a single-particle spectrum corresponds to the linear response of OC at $\omega = U$, which can constitute a convenient point for experimental realization [20].

If we consider OC in layered systems by using Eq. (7), the situation is more involved. Below we present the behavior of OC for three values of commensurability fields, i.e., $f = 1/2, 1/3, 1/4$ with different numbers of layers in the system and isotropic hopping $\eta = 1$. For $f = 1/2, 1/4$, the analytical formula for DOSc was derived in Ref. [20]. In Appendix D we give the solution for $f = 1/3$ in terms of complete elliptic integrals.

Figures 1–3 illustrate the great impact of restricted geometry on OC in the BHM when a strong magnetic field is present. In the crossover region for up to approximately ten layers we notice that such a slab geometry generates a rich, frequency-dependent behavior of the conductivity peaks. In the limit of several tens of layers three-dimensional behavior of the optical lattice subjected to the external uniform magnetic field in the z direction is recovered.

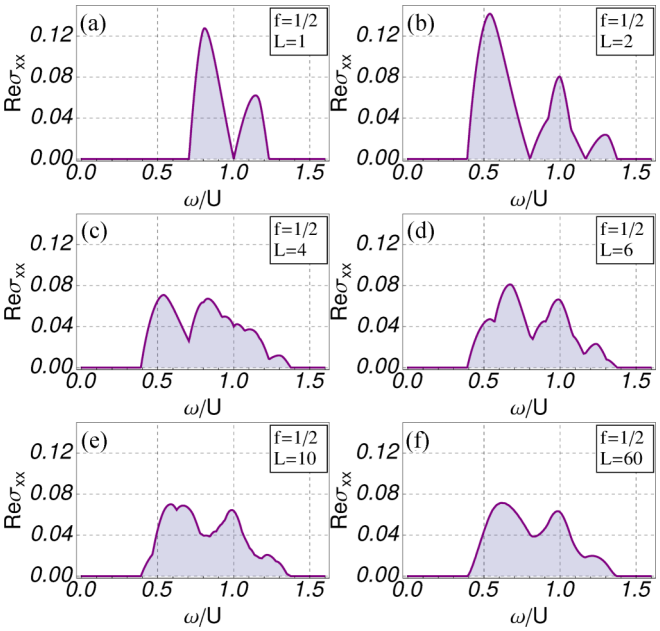

FIG. 1. (Color online) Frequency dependence of the optical conductivity in the Mott phase with $f = 1/2$ for the different number of layers (the case with $L = 1$ was calculated in Ref. [20]). The hopping parameter was chosen with the values $J/U = 0.03$ and $\eta = 1$ (isotropic case) and the conductivity is plotted in σ_Q unit (σ_Q is a quantum conductance). Figures are plotted for $n_0 = 1$ (the first lobe of the Mott-insulator phase).

B. Nonmonotonous behavior of optical conductivity

From Figs. 1–3 we can conclude that the amplitude of OC for a given frequency is a nonmonotonous function of the number of layers (a similar situation occurs as the amplitude of strong magnetic field is changed). To illustrate this dependence

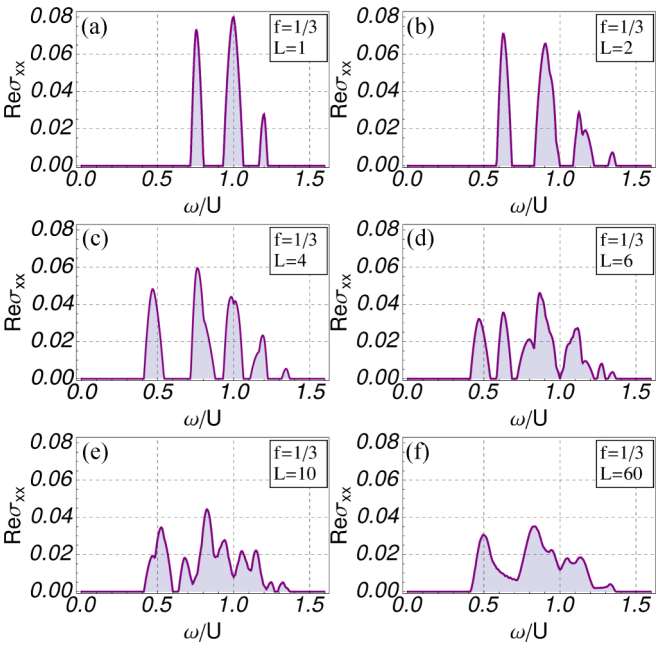

FIG. 2. (Color online) Analogous parameters as in Fig. 1 but with $f = 1/3$.

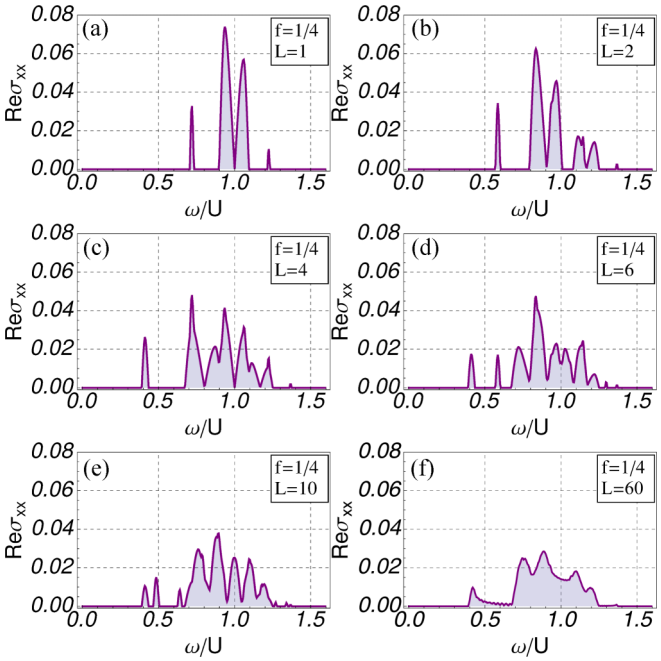

FIG. 3. (Color online) Analogous parameters as in Fig. 1 but with $f = 1/4$.

we plot it in Fig. 4 for a special point $\omega = U$. Interestingly, if the number of layers for $f = 1/2$ is more than one, we observe finite conductivity instead of its zero value in the pure two-dimensional system [see Figs. 1 and 4(a)]. This is in contrast to the cases of $f = 1/3$ and $1/4$. For $f = 1/3$ we observe insulating behavior for two, three, and six layers [Fig. 4(b)] however for a field $f = 1/4$ the conductivity vanishes for one, two, four, and eight layers [Fig. 4(c)]. All these nonmonotonous effects assigned to discrete structure disappear if the system is built of more than 10–13 layers and then we can treat it as a quasi-three-dimensional system (a similar observation in the context of phase boundary in BHM has been predicted in Ref. [11]).

Before we clarify why OC vanishes for a certain number of layers at $\omega = U$, we should pay attention to the physical information carried by the spectral functions included in OC. At the first step, it is very useful to make consideration in terms of weighted density of states (DOSc), Eq. (7), because DOSc provides information about the vanishing of OC, see also Eqs. (2)–(4). Moreover, to make the discussion more transparent, we focus separately on each component $\rho_q^\alpha(v + 2\eta\cos k_z, p)$ of the sum in Eq. (7), which is a two-dimensional DOSc defined in Eq. (5). The behavior of $\rho_q^\alpha(v + 2\eta\cos k_z, p)$ is very similar to that of the well-known single-particle density of states (DOS) [30], as we show for $f = 1/2, 1/3, 1/4$ in Fig. 5 and in Appendix C. Next, we use the fact that magnetic field is manifested in $\rho_q^\alpha(v + 2\eta\cos k_z, p)$ through the following: (i) appearance of additional gaps (its quantity depends on f); (ii) disappearance of density of states at one point if Dirac cones exist in the quasiparticle spectrum. Both effects are also clearly visible in the quasiparticle energy spectra [20] or in quasiparticle density of states (DOSq) in Figs. 5(c), 5(f), 5(i), 5(l). Moreover, for OC it means that spectra show characteristic peaks at the order of U. It is

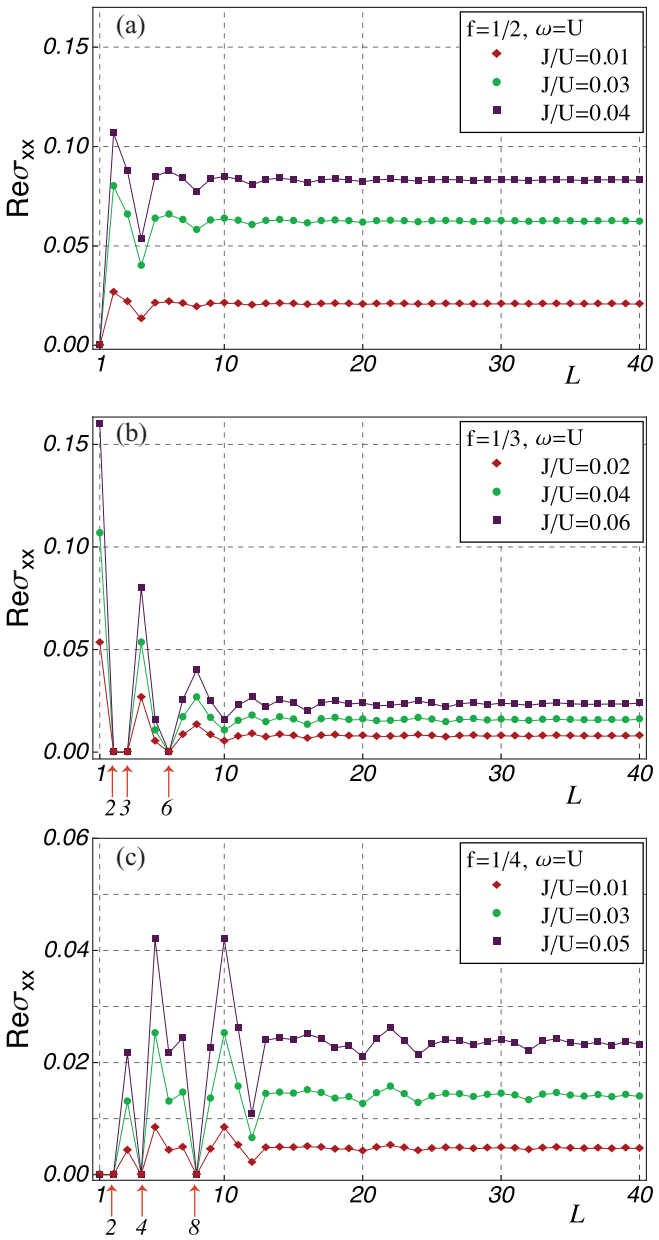

FIG. 4. (Color online) The optical conductivity dependent on the number of layers for the special point $\omega = U$ and different values of J/U. We assume the isotropic case of the hopping parameter, i.e., (a)–(c) $\eta = 1$ are plotted for $f = 1/2$, $f = 1/3$, and $f = 1/4$, respectively. We observe the insulator behavior for $L = 2$, 3, 6 and for $L = 1$, 2, 4, 8 numbers of layers for $f = 1/3$ and $f = 1/4$, respectively. In the case of the single-layer system see Ref. [20]. Conductivity is plotted in σ_Q unit and for $n_0 = 1$.

so, because the response of the system is directly related to the energy difference between quasiparticle and quasihole spectra [20]. Consequently, the observed peaks for different strengths of magnetic field f and different numbers of layers L could show very complex structure (as we present in Sec. III A). It should also be observed that in a two-dimensional system the energy difference between the points at which DOSq vanishes (because of Dirac cones), is equal to U, see Figs. 5(f) and 5(l), and exactly this property is responsible for the vanishing of OC at $\omega = U$ for $f = 1/2$ and $f = 1/4$ [20].

Finally, with the reference to the considerations from the above paragraph, we can explain why OC takes zero value for a certain number of layers and for arbitrary ω (further we focus on $\omega = U$). Namely, OC vanishes, when each argument $v + 2\eta \cos k_z$ of the function $\rho_q^\alpha(v + 2\eta \cos k_z, p)$ following from the sum Eq. (7) is equal to the energy E/J for which DOSc also vanishes because of the two effects given above. In other words, the multilayered structure introduces to DOSc an additional shift of energy scale, which for a given number of layers and a given ω could not give the electric response of the system, which is a direct consequence of subband structure of DOSc. In particular if we choose $\omega = U$, OC vanishes for $f = 1/2, 1/3, 1/4$ with a given number of layers listed in the first paragraph of this section. To see this more clearly let us consider the argument of DOSc, i.e., $v + 2\eta \cos k_z$. For $\omega = U$, we can precisely say that $v = 0$ or $v \gg 1$ in $v + 2\eta \cos k_z$ because of $v = u^{\pm}(\omega)$ in OC, which effectively gives $2\eta \cos k_z$ instead of $v + 2\eta \cos k_z$ (see more detailed discussion in the next paragraphs). Consequently, to illustrate why OC vanishes for a certain number of layers at $\omega = U$, we plot in Fig. 6 the distribution of $2\eta \cos k_z$ for different values of L in the background of the density plot of $\rho_q^\alpha(\omega/J, p)$, which explicitly shows the vanishing of components in the sum from Eq. (7) within a given number of layers L (red circles in Fig. 6).

Because of the fractal structure of DOS [32] and consequently of DOSc (see Fig. 5) it is difficult to give a simple explanation why OC vanishes for a given set of L. Moreover, it is the case not only for $\omega = U$ but for an arbitrary ω. What we can conclude is that the explanation of vanishing conductivity for $L > 1$ and $\omega = U$ in contrast to the one layered case needs also the gapped behavior of DOSc (in a two-dimensional system the responsibility for this takes only Dirac-like physics, see the second paragraph of this section and Ref. [20]). We also conclude that approximately for more than ten layers, the distribution of $v + 2\eta \cos k_z$ for a given set of k_z is too dense within the band so that OC could vanish (see Fig. 6).

C. Robustness of dynamical conductivity at the special point $\omega = U$

There is one important thing that we should point out here, namely OC for $\omega = U$ shows stable insulator behavior in the whole Mott area of the phase diagram. This happens for a given number of layers and p/q ratio as is presented in Fig. 4 using different parameters of J/U. To justify the stable insulator behavior of OC at $\omega = U$, we should again consider the argument of DOSc, i.e., $v + 2\eta \cos k_z$, see Eqs. (2)–(4) and (7), where $v = u^{\pm}(\omega)$ and here we analyze the isotropic case $\eta = 1$. Namely, when OC vanishes at $\omega = U$, the relevant dependence of OC on J/U is presented in $u^{\pm}(\omega)$, so then we consider the behavior of $u^{\pm}(\omega)$. First, we can notice that $u^{+}(\omega = U)$ is 0 [see Eq. (4)]. Consequently, the argument of DOSc is J/U independent and if conductivity vanishes we obtain stable insulatorlike behavior at $\omega = U$. For the opposite case, i.e., $\omega \neq U$, we have J/U dependence of DOSc [see Eq. (4)] and robustness of optical conductivity for this points is violated. Second, the value of $u^{-}(\omega)$ at any arbitrary ω is higher than the band width in DOSc and it does not contribute to OC. Finally, as follows from the above, the relevant argument of

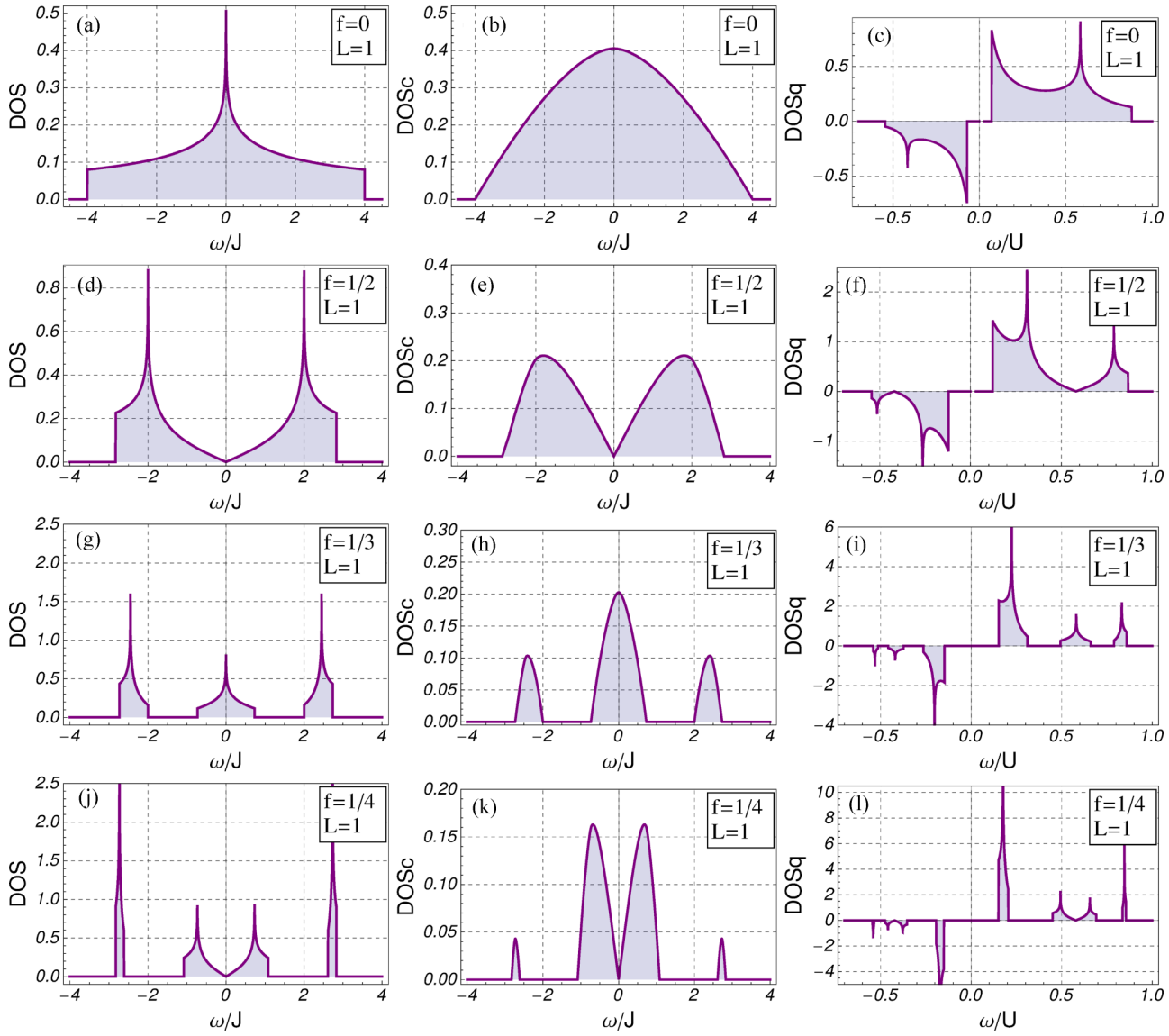

FIG. 5. (Color online) Frequency dependence ω of: (a), (d), (g), (j) the single-particle density of states (DOS); (b), (e), (h), (k) the weighted single particle density of states for conductivity (DOSc); and (c), (f), (i), (l) the quasiparticle density of states (DOSq). Plots are made for (a)–(c) $f = 0$; (d)–(f) $f = 1/2$; (g)–(i) $f = 1/3$; and (j)–(l) $f = 1/4$. For DOSq with $n_0 = 1$ in (c), (f), (i), (l) we use $J/U = 0.042, 0.057, 0.057, 0.055$, respectively.

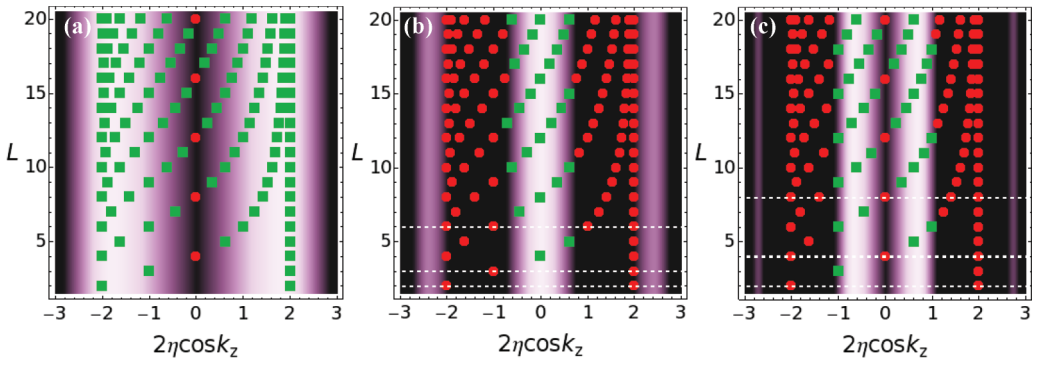

FIG. 6. (Color online) Distribution of $2\eta \cos k_z$ argument of the sum in Eq. (7) for $\omega = U$, $\eta = 1$ (red circles and green squares) and for different values of L within density plot of DOSc, i.e., $\rho_q^\alpha(\omega/J, p)$. Red circle appears if $\rho_q^\alpha(2\eta \cos k_z, p) = 0$, green square appears if $\rho_q^\alpha(2\eta \cos k_z, p) \neq 0$. (a) corresponds to $f = 1/2$, (b) $f = 1/3$, and (c) $f = 1/4$. (b) and (c) explicitly show the vanishing components of the sum in Eq. (7) for the number of layers $L = 2, 3, 6$ with $f = 1/3$ and for $L = 2, 4, 8$ with $f = 1/4$ (dashed white lines).

DOSc at $\omega = U$ is J/U independent and consequently OC is robust as well, which we wanted to prove.

Moreover for the analyzed cases in which $f < 1/2$ the range of numbers of layers for which OC could disappear can be estimated from

$$\mathrm{Re}\,\sigma_{xx}^{\mathbf{A}_0}(U) = 0 \quad \text{for} \quad \frac{1}{f} \geq \frac{L}{2} \geq 1, \tag{8}$$

where the number of layers for which the insulating state emerges can be calculated from the simple general formula ($L > 2$):

$$L|_{\mathrm{Re}\,\sigma_{xx}^{\mathbf{A}_0}(\mathrm{U})=0} = \frac{n}{f} \tag{9}$$

and depends only on the inverse of flux density f^{-1} (see Fig. 4) with $n = 1,2,\ldots$ being integer. Although, the validation of Eqs. (8) and (9) for the other values than $f = 1/3, 1/4$ is an open question, we should point out here that in general many other properties in the strongly correlated systems carry f dependence [33] so it seems valuable to give here such a simple estimation.

D. Anisotropy effects

The robust insulator behavior of OC for $\omega = U$ (see Fig. 4) in the Mott phase is stable for the isotropic lattice. This is in contrast to the case when we include anisotropic effects easily controlled in optical lattices. Namely, for reduced hopping amplitude in the z direction, the finite conductivity emerges for a special value of the anisotropy parameter $\eta = \eta_c$. The critical η_c depends on the number of layers in the system, but does not depend on the ratio J/U, i.e., this value is also robust in the whole Mott phase. We present this behavior in Fig. 7.

This robustness of OC down to η_c, again could be explained using $u^{\pm}(\omega) + 2\eta\cos k_z$, i.e., the argument of DOSc and its connection to the single-particle DOS (see Sec. III B). Namely, $u^{\pm}(\omega)$ for $\omega = U$ is unimportant because of its zero value for the $+$ index and a too high value for the $-$ index. Then we obtain that the relevant component of the sum in Eq. (7) has the form $\rho_q^{\alpha}(2\eta\cos k_z, p)$ whose argument does not depend on J/U but only on k_z and η. The summation over k_z causes different distribution of $2\eta\cos k_z$ with given k_z, which was discussed in Sec. III C. Here, we consider the influence of η. It is important to note that the values of $2\eta\cos k_z$ for $\eta \ll 1$ and different k_z concentrate around 0, which implies nonzero DOSc for energy values in range of $2\eta\cos k_z$. In other words, this happens because the nonzero subbands structure exists around this point in DOSc (see Fig. 5 and Appendix C) and as a consequence, for a given f there exists a critical value η_c for which the distribution of $2\eta\cos k_z$ coincides with the energy range where DOSc does not disappear and OC shows metallic-like behavior. Finally, from the above considerations, we see that η from η_c to 1 gives the robust behavior of vanishing OC in terms of J/U.

Surprisingly, we also observe in Fig. 7(b) that for $L = 2$, 4, and 8, when a layered system is subjected to a magnetic field $f = 1/4$, there exists a maximal value of OC at $\omega = U$ for given J/U. This does not happen for the $f = 1/3$ case in which the η dependence of OC is monotonous [see Fig. 7(a)]. This fact can be simply explained knowing that for $f = 1/4$, in the $\eta \to 0$ limit OC does not have any weight at $\omega = U$ [20]. This is in contrast to $f = 1/3$ case for which the weight of OC at $\omega = U$ is finite.

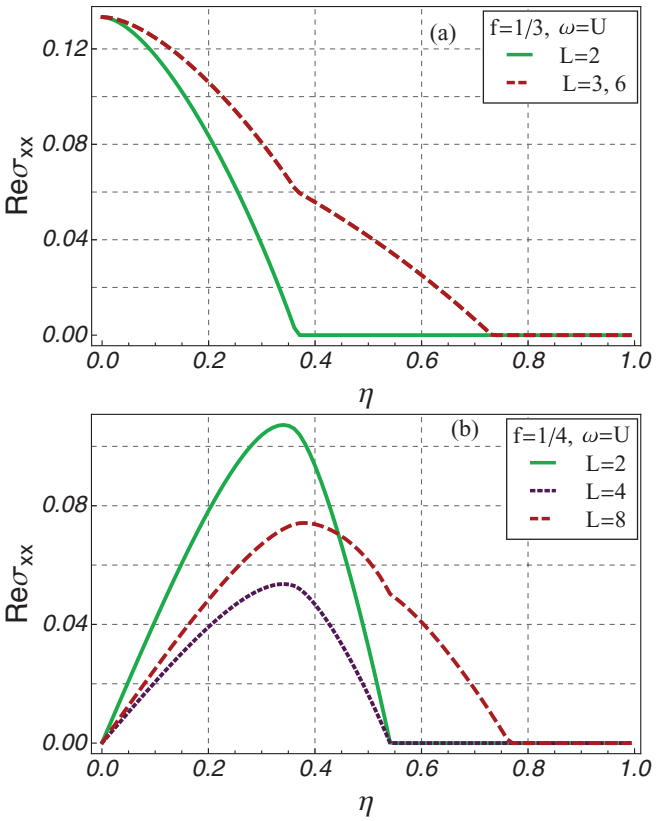

FIG. 7. (Color online) The anisotropy dependence of the optical conductivity for the point $\omega = U$ and the special number of layers for which OC is robust with respect to the insulator state (see Fig. 4). Here we take $J/U = 0.05$. Conductivity is plotted in σ_Q unit and for $n_0 = 1$.

E. Critical correspondence between the number of layers and single-particle subbands

As follows from the previous study [20,28], the zero-temperature three-dimensional system does not show the critical conductivity σ_c at the Mott-insulator–superfluid phase boundary, which should be contrasted to the two-dimensional case. Here we show that σ_c in the 2D to 3D discrete crossover region does not abruptly vanish but is rather gradually suppressed by the introduction of additional layers to the system. In order to enhance the σ_c behavior, we include a strong magnetic field (e.g., $f = 1/3$ gives approximately three times larger value of σ_c [20,34], which can be useful for experimental realization).

To describe the impact of layered structure under a strong magnetic field on the critical conductivity, it is convenient to denote this critical quantity by $\sigma_{c,f}(L)$. Next, we assume that the MI-SF transition is of second order and we apply the Ginzburg-Landau theory for the lowest subband of our system [20]. This lowest subband contains q lowest-energy modes in the first magnetic Brillouin zone with minima at $\mathbf{k} = \mathbf{Q}$. It is important to note that making an expansion around $\mathbf{Q}$

we choose from the discrete set of k_z the value $k_z = 0$ (because of the lowest value of quasiparticle energy at this point). Then at the MI-SF phase boundary, we get the following expression

$$\sigma_{c,f}(L) = \frac{q}{L}\sigma^*, \tag{10}$$

where $\sigma^* = \pi\sigma_Q/8$ and q is a number of Hofstadter subbands for the single-particle spectrum. This implies $\sigma_{c,f}(L) \sim 1/L$. Therefore we simply see that $\sigma_{c,f}(L)$ in the layered system goes to zero when $L \to \infty$, which is consistent with vanishing of this quantity in the limit of a three-dimensional system [20,28]. Within the above approximation, it is interesting to point out that critical conductivity in a layered system with magnetic field strength f is the same as in the two-dimensional case without a magnetic field when the experiment is performed for $L = q$, i.e., then $\sigma_{c,f}(L = q) = \sigma^*$. In other words, the critical conductivity does not change, if the following correspondence appears: the number of layers L and the number of Hofstadter subbands q are the same. This correspondence between L and q [and as well as Eq. (10)] should be at least valid for $p \approx 1$ [20] and for the discrete set of k_z in the first Brillouin zone for which the continuous approximation for variable k_z is not appropriate. The latter condition is needed because for continuous approximation of variable k_z we have $L \to \infty$, i.e., it recovers the three-dimensional system and then critical conductivity simply vanishes, which is the well-known behavior [20,28]. As far as the first condition is concerned, i.e., $p \approx 1$ it seems that Eq. (10) is valid at least for small value of p close to 1. We based this assumption on the previous calculations for $p = 1$ and $L = 1$ [20], which are in good agreement with analytical [35,36], numerical [34,37], and experimental data [38,39]. For other values of p the validation of Eq. (10) is still an open question, e.g., for $L = 1$, $\sigma_{c,f}(L)$ could be inversely proportional to p, like a critical conductivity in a two-dimensional Josephson junction [39], but this is difficult to assess because of a large error margin in experimental data where additional effects such as disorder of the system or temperature play an important role.

IV. EXPERIMENTAL SETUPS OF THE LAYERED OPTICAL LATTICE

Recently, the authors of Ref. [21] have proposed a method that allows a direct investigation of OC on an optical lattice by using phase modulation of the lattice potential. Namely, they have shown that the current-current correlation function is proportional to the energy absorption rate $R_{\mathrm{PM}}(\omega)$ and the results presented in Secs. III A–D could be simply translated to this quantity, i.e., by multiplying $\mathrm{Re}\sigma_{xx}$ with the power-dependent ω, which only changes the weight of OC, leaving the quality of its behavior intact. Moreover, very recently, another experimental setup to measure OC has been proposed by the authors of Ref. [22]. The key idea presented in Ref. [22] relies on making use of the oscillatory motion of harmonic trap.

In order to study two-layered systems in a highly controllable way we propose to make use of a superlattice potential along the z direction, which is created by superimposing two standing waves with wave vector k_z and k_{lz}, with $k_z = 2k_{lz}$. The resulting lattice potential is described by $V(z) = V_{lz}\sin^2(k_{lz}z + \varphi) + V_z\sin^2(k_z z)$ and the corresponding lattice depths V_{lz}, V_z as well as the relative phase φ can be controlled fully independently in experiments. For $\varphi = \pi/4$ and $V_{lz} \geq V_z$ a symmetric double-well potential can be realized where tunneling between neighboring double wells is suppressed and atoms can only tunnel within a double well [40,41]. Together with the usual two-dimensional lattice in the xy plane a stack of layers is generated where only two layers at a time are coupled, which allows us to simulate the physics of bilayered systems. Moreover, the repeated structure of two layers should lead to an amplification of the expected physical effects. This method could allow investigation of many interesting phenomena, not available so far in optical lattices [42–47].

To realize n-layer potentials, a single wavelength lattice in the z direction can be used. The number of layers can then be reduced to the desired amount by using a box-type potential [48] in the vertical direction.

Moreover, we notice that in current setups a major limitation to observe features described in this manuscript is the inhomogeneity of systems. Both in radial (planar) and vertical directions, an underlying confining potential is typically present to trap the atoms or due to the finite size of the lattice beams. This problem could again be used by compensating the harmonic confining potentials and provide box-type hard walls [48] also in radial direction.

However, if harmonic nonuniformity of underlying trapping potential in planar and vertical direction is present [i.e., $V_{\mathrm{trap}}(r) = m\omega_r^2 r^2/2$ and $V_{\mathrm{trap}}(z) = m\omega_z^2 z^2/2$, respectively], the effects of one type should be visible in Figs. 1–3 (we neglect here nonuniformity of tunneling amplitude). Namely, the harmonic trap introduces a superfluid phase to the system, which surrounds the atoms in the Mott-insulator state, or superfluidity could appear in the middle of the atomic cloud [49,50]. Consequently, in the gapped region of Figs. 1–3 for frequencies $\omega \ll U$, low-energy excitations emerge [22]. But the peaks structure in the frequency region $\omega \sim U$ should be robust against the harmonic trap (so vanishing of OC at $\omega = U$ as well, see Sec. III B). This happens because OC in the Mott-insulator phase, Eqs. (2)–(7), does not depend on chemical potential and if local density approximation (LDA) to chemical potential is used, i.e., $\mu(r,z) = \mu - V_{\mathrm{trap}}(r) - V_{\mathrm{trap}}(z)$, then the response of the system unaffected by trapping potential is generated (similar robustness of response to the trapping in the Mott-insulator phase was obtained by the authors of Ref. [51]). Moreover, we should mention here again that the effects of trapping in the z direction will be prominent only if we apply to the system, for instance, a double-well potential because of its repeated structure. It does not happen for the box potential, but then it gives a weaker response signal originating only from one realization of bilayer system at the same time.

V. SUMMARY

Using the analytical approach we show the behavior of the optical and the critical conductivity in the Mott phase for the zero-temperature limit, when the additional layers are attached to the system. For the reason of complex dynamics behavior in BHM in strong uniform magnetic field we consider $f = 1/2$, $1/3$, and $1/4$ magnetic flux ratio. Frequency-dependent conductivity reveals rich insulator-conductor behavior, which

could be of interest for future possible applications. Especially, we show that for $f = 1/3$ ($f = 1/4$) optical conductivity abruptly changes from metallic to insulating for the frequency corresponding to the on-site boson interaction energy with two, three, six (one, two, four, eight) layers. In the case of $f = 1/2$, metallic behavior emerges when the number of layers is higher than one. Interestingly, such an insulating behavior is robust in the whole range of parameters in the Mott phase and we estimate exactly how many of slabs we must add to achieve zero value of the optical conductivity. The three-dimensional limit is reached for number of layers more than 10–13 and depends on the flux density.

Additionally, we investigate the anisotropic kinetic energy in perpendicular to the layers direction. We show that the critical value of anisotropy for which finite conductivity appears is also robust in the Mott phase (this happens for frequency corresponding to the on-site boson interaction). Moreover, for $f = 1/3$ there exists a maximum value of conductivity for a given anisotropy amplitude.

We consider also the critical behavior of the conductivity on the phase boundary. This shows that it gradually vanishes starting from 2D and approaching the 3D system. Moreover including commensurate magnetic field effects we show the critical correspondence between the number of Hofstadter subbands and the number of layers.

To confirm our predictions we propose the experimental setup for creation of highly controllable simulators of the layered systems in optical lattices. This also could give the opportunity to simulate the standard condensed matter devices, including, e.g., bilayer systems, where such a restricted geometry plays important role.

ACKNOWLEDGMENTS

We thank Professor R. Micnas for his interest and useful comments regarding the manuscript. We also are grateful to M. Aidelsburger for careful reading our manuscript and comments concerning the experimental setup. The work was supported by (Polish National Science Center Grant No. DEC-2011/01/D/ST2/02019.

APPENDIX A: USEFUL EXPRESSION IN THE OPTICAL CONDUCTIVITY EQUATION

The weight presented in Eq. (3) is defined as follows

$$z_q^\alpha(\mathbf{k};p) = \frac{E_q^{\alpha+}(\mathbf{k};p) + \mu + U}{E_q^{\alpha+}(\mathbf{k};p) - E_q^{\alpha-}(\mathbf{k};p)}, \tag{A1}$$

where

$$E_q^{\alpha\pm}(\mathbf{k};p) = \frac{\epsilon_q^\alpha(\mathbf{k};p)}{2} - \mu + U\left(n_0 - \frac{1}{2}\right) \pm \frac{1}{2}\Delta_q^\alpha(\mathbf{k};p), \tag{A2}$$

$$\Delta_q^\alpha(\mathbf{k};p) = \sqrt{\left[\epsilon_q^\alpha(\mathbf{k};p)\right]^2 + 4\epsilon_q^\alpha(\mathbf{k};p)U\left(n_0 + \frac{1}{2}\right) + U^2}. \tag{A3}$$

APPENDIX B: DENSITY OF STATES FOR THE CONDUCTIVITY IN THE LAYERED SYSTEMS

For additional layers in the z direction the single-particle dispersion relation has a form $\epsilon_q^\alpha(\mathbf{k};p) - 2J_z\cos k_z$ and this dispersion implies that DOSc has a form

$$\begin{aligned}\rho_{q,3D}^\alpha(v;p) &= \frac{1}{NL}\sum_{\mathbf{k}k_z}\left[\partial_{k_x}\left(\epsilon_q^\alpha(\mathbf{k};p) - 2J_z\cos k_z\right)\right]^2 \\ &\quad\times\delta\left(v - \epsilon_q^\alpha(\mathbf{k};p)/J + 2\eta\cos k_z\right) \\ &= \frac{1}{L}\sum_{k_z}\int_{-\infty}^{\infty} dx\,\rho_q^\alpha(x;p)\delta(v - x + 2\eta\cos k_z) \\ &= \frac{1}{L}\sum_{k_z}\rho_q^\alpha(v + 2\eta\cos k_z;p).\end{aligned}$$

APPENDIX C: DENSITY OF STATES: GENERAL FORMULAS

For the analysis presented in this paper, it is useful to consider three types of density of states, namely:

(i) Single-particle density of states (DOS)

$$D_q^\alpha(\omega;p) = \frac{1}{N}\sum_{\mathbf{k}}\delta\left(\omega/J - \epsilon_q^\alpha(\mathbf{k};p)/J\right), \tag{C1}$$

which for two dimensions is plotted in Figs. 5(a), 5(d), 5(g), 5(j) for different strengths of magnetic field f (see also Ref. [30]),

(ii) Weighted single-particle density of states for conductivity (DOSc), see Eq. (5) (two-dimensional lattice) and Eq. (7) (multilayered lattice). DOSc for two dimensions is plotted in Figs. 5(b), 5(e), 5(h), 5(k) with different f (see also Ref. [52] with $f = 0$ case),

(iii) Quasiparticle density of states (DOSq) (for two dimensions)

$$\rho_{q,MI}^\alpha(\omega;p) = -\frac{1}{\pi}\frac{1}{N}\sum_{\mathbf{k}}\mathrm{Im}\mathcal{G}_{\alpha\alpha}^d(\mathbf{k},\omega + i0^+), \tag{C2}$$

where

$$\begin{aligned}\mathcal{G}_{\alpha\alpha}^d(\mathbf{k},i\omega_n) &= \frac{G_0(i\omega_n)}{1 - \epsilon_q^\alpha(\mathbf{k};p)G_0(i\omega_n)} \\ &= \frac{z_q^\alpha(\mathbf{k};p)}{i\omega_n - E_q^{\alpha+}(\mathbf{k};p)} + \frac{1 - z_q^\alpha(\mathbf{k};p)}{i\omega_n - E_q^{\alpha-}(\mathbf{k};p)},\end{aligned} \tag{C3}$$

and where $\mathcal{G}_{\alpha\alpha}^d(\mathbf{k},i\omega_n)$ is a Mott-insulator Green's function. For the multilayered case, the following substitution should be done $\epsilon_q^\alpha(\mathbf{k};p) \to \epsilon_q^\alpha(\mathbf{k};p) - 2J_z\cos k_z$. DOSq for one layer is plotted in Figs. 5(c), 5(f), 5(i), 5(l) with different f.

APPENDIX D: TWO-DIMENSIONAL DENSITY OF STATES FOR THE CONDUCTIVITY IN A STRONG MAGNETIC FIELD

The single-particle spectrum for $f = 1/3$ consists of three subbands, namely $\pm 2\sqrt{2}\cos[\pi/6 \pm \arctan[g(k_x,k_y)]/3]$ and

$2\sqrt{2}\sin[\frac{1}{3}\arctan[g(k_x,k_y)]]$ where

$$g(k_x,k_y)=\frac{\cos(k_x)+\cos(k_x)}{\sqrt{8-[\cos(k_x)+\cos(k_x)]^2}}. \tag{D1}$$

The density of states calculated from Eq. (5) has a form

$$\rho_3^{\alpha}(E;1)=\frac{8\sqrt{2}}{\pi^2}\sum_{m\in\{0,1\}}\Theta_{\alpha,m}\Omega[x_m(E)] \times\frac{\left|\sin\left(\frac{\pi}{6}\pm\frac{1}{3}\arctan\frac{x_m(E)}{\sqrt{32-(x_m(E))^2}}\right)\right|}{\sqrt{32-[x_m(E)]^2}}, \tag{D2}$$

$$\rho_3^{\alpha}(E;1)=\frac{8\sqrt{2}}{\pi^2}\sum_{m\in\{0,1\}}\Theta_{\alpha,m}\Omega[y_m(E)] \times\frac{\left|\cos\left(\frac{1}{3}\arctan\frac{y_m(E)}{\sqrt{32-(y_m(E))^2}}\right)\right|}{\sqrt{32-[y_m(E)]^2}}, \tag{D3}$$

where sign $\pm$ depends on α and $\Theta_{\alpha,m}$ is a step function with respect to a given subband α and index m. Moreover in Eqs. (D2) and (D3) we introduce the following functions

$$\Omega(x)=\mathcal{E}\left(\sqrt{1-\left(\frac{x}{4}\right)^2}\right)-\left(\frac{x}{4}\right)^2\mathcal{K}\left(\sqrt{1-\left(\frac{x}{4}\right)^2}\right), \tag{D4}$$

$$x_m(E)=(-1)^m 4\sqrt{\frac{2\tan^2\left[3\arccos\left(\frac{E}{2\sqrt{2}}\right)-\frac{\pi}{2}\right]}{1+\tan^2\left[3\arccos\left(\frac{E}{2\sqrt{2}}\right)-\frac{\pi}{2}\right]}}, \tag{D5}$$

$$y_m(E)=(-1)^m 4\sqrt{\frac{2\tan^2\left(3\arcsin\frac{E}{2\sqrt{2}}\right)}{1+\tan^2\left(3\arcsin\frac{E}{2\sqrt{2}}\right)}}, \tag{D6}$$

where $\mathcal{K}(x)$ and $\mathcal{E}(x)$ are complete elliptic integrals of the first and second kinds, respectively.

[1] M. Olshanii, Phys. Rev. Lett. **81**, 938 (1998).
[2] D. S. Petrov and G. V. Shlyapnikov, Phys. Rev. A **64**, 012706 (2001).
[3] S. Burger, F. S. Cataliotti, C. Fort, P. Maddaloni, F. Minardi, and M. Inguscio, Europhys. Lett. **57**, 1 (2002).
[4] T. Kinoshita, T. Wenger, and D. S. Weiss, Science (N.Y.) **305**, 1125 (2004).
[5] B. Paredes, A. Widera, V. Murg, O. Mandel, S. Fölling, I. Cirac, G. V. Shlyapnikov, T. W. Hänsch, and B. Immanuel, Nature (London) **429**, 277 (2004).
[6] T. Stöferle, H. Moritz, C. Schori, M. Köhl, and T. Esslinger, Phys. Rev. Lett. **92**, 130403 (2004).
[7] E. Haller, M. Gustavsson, M. J. Mark, J. G. Danzl, R. Hart, G. Pupillo, and H.-C. Nägerl, Science (N.Y.) **325**, 1224 (2009).
[8] L. Tarruell, D. Greif, T. Uehlinger, G. Jotzu, and T. Esslinger, Nature (London) **483**, 302 (2012).
[9] V. Pietilä, D. Pekker, Y. Nishida, and E. Demler, Phys. Rev. A **85**, 023621 (2012).
[10] T. P. Polak and T. K. Kopeć, Ann. Phys. (N.Y.) **17**, 947 (2008).
[11] T. A. Zaleski and T. P. Polak, Phys. Rev. A **83**, 023607 (2011).
[12] M. Kanász-Nagy, E. A. Demler, and G. Zaránd, arXiv:1401.5798.
[13] P. Krüger, Z. Hadzibabic, and J. Dalibard, Phys. Rev. Lett. **99**, 040402 (2007).
[14] Q. Sun, L. Wen, W.-M. Liu, G. Juzeliūnas, and A.-C. Ji, arXiv:1403.4338.
[15] M. Greiner, O. Mandel, T. Esslinger, T. W. Hänsch, and I. Bloch, Nature (London) **415**, 39 (2002).
[16] T. Schwartz, G. Bartal, S. Fishman, and M. Segev, Nature (London) **446**, 52 (2007).
[17] M. Aidelsburger, M. Atala, S. Nascimbène, S. Trotzky, Y.-A. Chen, and I. Bloch, Phys. Rev. Lett. **107**, 255301 (2011).
[18] M. Aidelsburger, M. Atala, M. Lohse, J. T. Barreiro, B. Paredes, and I. Bloch, Phys. Rev. Lett. **111**, 185301 (2013).
[19] H. Miyake, G. A. Siviloglou, C. J. Kennedy, W. C. Burton, and W. Ketterle, Phys. Rev. Lett. **111**, 185302 (2013).
[20] A. S. Sajna, T. P. Polak, and R. Micnas, Phys. Rev. A **89**, 023631 (2014).
[21] A. Tokuno and T. Giamarchi, Phys. Rev. Lett. **106**, 205301 (2011).
[22] Z. Wu, E. Taylor, and E. Zaremba, arXiv:1406.3358.
[23] D. Jaksch, C. Bruder, J. I. Cirac, C. W. Gardiner, and P. Zoller, Phys. Rev. Lett. **81**, 3108 (1998).
[24] K. Sengupta and N. Dupuis, Phys. Rev. A **71**, 033629 (2005).
[25] T. P. Polak and T. K. Kopeć, Phys. Rev. B **76**, 094503 (2007).
[26] S. Sinha and K. Sengupta, Europhysics Lett. **93**, 30005 (2011).
[27] M. P. A. Fisher, G. Grinstein, and S. M. Girvin, Phys. Rev. Lett. **64**, 587 (1990).
[28] A. P. Kampf and G. T. Zimanyi, Phys. Rev. B **47**, 279 (1993).
[29] Y. J. Lin, R. L. Compton, K. Jiménez-García, J. V. Porto, and I. B. Spielman, Nature (London) **462**, 628 (2009).
[30] Y. Hasegawa, P. Lederer, T. M. Rice, and P. B. Wiegmann, Phys. Rev. Lett. **63**, 907 (1989).
[31] T. P. Polak and T. K. Kopeć, Phys. Rev. A **79**, 063629 (2009).
[32] D. R. Hofstadter, Phys. Rev. B **14**, 2239 (1976).
[33] M. M. Maśka, Phys. Rev. B **66**, 054533 (2002).
[34] M. C. Cha and S. M. Girvin, Phys. Rev. B **49**, 9794 (1994).
[35] E. Granato and J. M. Kosterlitz, Phys. Rev. Lett. **65**, 1267 (1990).
[36] G. M. Grason and R. F. Bruinsma, Phys. Rev. Lett. **97**, 027802 (2006).
[37] M.-C. Cha, M. P. A. Fisher, S. M. Girvin, M. Wallin, and A. P. Young, Phys. Rev. B **44**, 6883 (1991).
[38] H. S. J. van der Zant, L. J. Geerligs, and J. E. Mooij, EPL **19**, 541 (1992).
[39] H. S. J. van der Zant, W. J. Elion, L. J. Geerligs, and J. E. Mooij, Phys. Rev. B **54**, 10081 (1996).
[40] J. Sebby-Strabley, M. Anderlini, P. S. Jessen, and J. V. Porto, Phys. Rev. A **73**, 033605 (2006).
[41] M. Anderlini, P. J. Lee, B. L. Brown, J. Sebby-Strabley, W. D. Phillips, and J. V. Porto, Nature (London) **448**, 452 (2007).
[42] M. Kellogg, J. P. Eisenstein, L. N. Pfeiffer, and K. W. West, Phys. Rev. Lett. **93**, 036801 (2004).
[43] S. V. Morozov, K. S. Novoselov, M. I. Katsnelson, F. Schedin, D. Elias, J. A. Jaszczak, and A. K. Geim, Phys. Rev. Lett. **100**, 016602 (2008).

[44] W. Bao, Z. Zhao, H. Zhang, G. Liu, P. Kratz, L. Jing, J. Velasco, D. Smirnov, and C. N. Lau, Phys. Rev. Lett. **105**, 246601 (2010).
[45] S. Das Sarma, E. H. Hwang, and E. Rossi, Phys. Rev. B **81**, 161407 (2010).
[46] A. S. Mayorov, D. C. Elias, M. Mucha-Kruczynski, R. V. Gorbachev, T. Tudorovskiy, A. Zhukov, S. V. Morozov, M. I. Katsnelson, V. I. Fal'ko, A. K. Geim *et al.*, Science (N.Y.) **333**, 860 (2011).
[47] J. Velasco, L. Jing, W. Bao, Y. Lee, P. Kratz, V. Aji, M. Bockrath, C. N. Lau, C. Varma, R. Stillwell *et al.*, Nature Nanotech. **7**, 156 (2012).
[48] A. L. Gaunt, T. F. Schmidutz, I. Gotlibovych, R. P. Smith, and Z. Hadzibabic, Phys. Rev. Lett. **110**, 200406 (2013).
[49] W. S. Bakr, A. Peng, M. E. Tai, R. Ma, J. Simon, J. I. Gillen, S. Fölling, L. Pollet, and M. Greiner, Science (N.Y.) **329**, 547 (2010).
[50] J. F. Sherson, C. Weitenberg, M. Endres, M. Cheneau, I. Bloch, and S. Kuhr, Nature (London) **467**, 68 (2010).
[51] S. D. Huber, E. Altman, H. P. Büchler, and G. Blatter, Phys. Rev. B **75**, 085106 (2007).
[52] L. Belkhir and M. Randeria, Phys. Rev. B **49**, 6829 (1994).